USAGE OF PARTICLE SWARM OPTIMIZATION IN DIGITAL IMAGES SELECTION FOR MONKEYPOX VIRUS PREDICTION AND DIAGNOSIS

Akshaya Kumar Mandal* and Pankaj Kumar Deva Sarma

Department of Computer Science, Assam University
Assam, Silchar 788011, Assam, India

Corresponding author: akshayacs207@gmail.com*, pankajgr@rediffmail.com

ABSTRACT

Identifying skin diseases by using digital images of skin that are also automated, efficient, and accurate is critical for biomedical image analysis. Many researchers have developed numerous machine-learning techniques for the prediction and diagnosis of various diseases that help clinicians identify infections early and provide crucial data for virus management. In this work, we use the inherent attributes of Particle Swarm Optimization (PSO), such as exploration and exploitation, to identify images for monkeypox virus prediction and diagnosis. Alongside, monkeypox, chickenpox, smallpox, cowpox, measles, tomato flu, and normal skin images were all considered in this study for monkeypox virus prediction and diagnosis. We collect photos from the International Skin Imaging Collaboration (ISIC) for analysis and experimentation purposes. Finally, we compare the proposed model Particle Swarm Optimization- Monkeypox Virus (PSOMPX) for monkeypox virus identification with four distinct pre-trained deep learning models (e.g., VGG16, ResNet50, InceptionV3, and Ensemble). Then we use four performance evaluation metrics—accuracy, precision, recall, and F1 score—to evaluate the model and analyze the outcomes of experiments. The experimental results obtained through the PSOMPX model significantly outperform other models due to its numerous traits.

Keywords: Monkeypox Virus; PSOMPX; Digital image selection; Skin lesion; Biomedical image; PSO.

1.0 INTRODUCTION

The infectious virus that causes the illness is an Orthopoxvirus, which is responsible for causing monkeypox. It was named "monkeypox virus" after being discovered in a monkey at a Danish research Centre in 1959 [1]. A young infant was admitted into the hospital with symptoms similar to smallpox in 1970 in the Republic of Congo, resulting in the confirmation of the first human case of this virus [2].It spreads to humans when infected people or contaminated materials come into contact with them [1]. It first started in the African region, but it has lately spread to over 106 nations, with 80,064 confirmed cases and 214 deaths as of October 5, 2022 [3, 4]. The monkeypox virus presently has two known varieties: one from Central Africa and other from West Africa. Because the monkeypox virus is now untreatable, so vaccine development is the only possible way of treatment. Monkeypox is commonly diagnosed using the polymerase chain reaction (PCR) technique or skin lesion test by electron microscope (Laboratory test). The most reliable approach for detecting viruses is PCR, and it has recently been used to diagnose COVID-19 [5, 6]. Accurate skin detection plays a critical role in various medical applications, including dermatology, and skin cancer detection. Despite significant advancements in image processing techniques, achieving high accuracy remains a persistent challenge. While existing methods have demonstrated commendable performance, there exists a demand for innovative approaches that can surpass current benchmarks. In this paper, we propose the utilization of bio-inspired methods to enhance the accuracy of skin detection algorithms, leveraging the inherent efficiency and adaptability of biological systems. The bio-inspired PSO-based approaches may assist in the identification of viruses through digital image processing and analysis.

The medical image analysis research projects have used a variety of artificial intelligence (AI) techniques over the last ten years, most notably deep learning approaches (for example, organ positioning [7, 8 and 9], identification of organ abnormalities [9,10], finding gene mutations [11], classifying cancer [12, 13], and staging [14]). Notably, AI algorithms have lately been crucial in the diagnosis and severity assessment of COVID-19 employing multimodal medical imaging (e.g., CT imaging, X-ray of the chest, and ultrasonography of the chest [14, 15 and 16]). This achievement inspires the scientific community to employ AI approaches to diagnose monkeypox from patient electronic skin photos. It is widely acknowledged that semi-supervised or supervised AI techniques are based on data, necessitating much information to design AI systems efficiently. In conclusion, monkeypox virus prediction and diagnosis through bio-inspired image recognition techniques involves leveraging computational models inspired by biological processes to analyze images of skin lesions associated

with the virus [17, 18]. By mimicking the visual processing mechanisms found in nature, such as neural networks or Swarm intelligence approaches, these techniques can efficiently identify patterns indicative of monkeypox infection through skin image. The machine learning algorithms and these systems can learn from vast datasets [19] of labeled images to accurately predict the presence of the virus based on characteristic features in the lesions. Additionally, bio-inspired algorithms allow for the development of robust diagnostic tools capable of quickly and accurately identifying monkeypox cases, aiding healthcare professionals in timely interventions and containment efforts.

2.0 RELATED WORKS

In this section, relevant research on automated skin lesion diagnostics, various PSO approaches, and existing strategies for feature selection in deep learning classifiers is discussed.

Tharangini et al. [20] proposed a computer-based particle swarm optimization method for early detection of skin cancer. Their approach involved processing dermoscopic images using various image processing techniques, with segmentation being a key step to separate malignant skin from healthy skin. They applied a Gray Level Co-occurrence Matrix (GLCM) to extract unique characteristics from the segmented images. These features were then used to classify the images as either malignant or non-cancerous. According to their findings, their proposed method demonstrated higher accuracy in diagnosing skin cancer compared to existing approaches.

Teck et al. [21] introduced an adaptive skin cancer detection method based on dermoscopic images, which enhances features through a variant of the PSO approach. They evaluated their model using different skin lesions from UCI datasets, and empirical results indicated improved performance attributed to their proposed techniques. To assess the efficacy of their PSO method, they compared the results using the Wilcoxon rank sum test against ten traditional search techniques and a hybrid PSO variants, particularly for addressing challenges in mathematical optimization and optimal feature selection across diverse settings.

Guan-Chun Luh [22] suggested utilizing multi-objective PSO to determine optimal threshold ranges for components in RGB-CbCrCg color spaces of skin images. The performance of this method was evaluated using the ECD database, showing superiority over fixed threshold RGB and other contemporary strategies.

Sitaula et al. [23] introduced deep learning-based pre-trained approach for identifying the monkeypox virus. They employed transfer learning to compare thirteen different pre-trained learning algorithms on a monkeypox dataset and selected effective models to enhance overall performance through ensemble methods. However, their work faces two significant limitations. Firstly, the dataset size is relatively small; suggesting that incorporating more data could further improve performance. Secondly, their AI technique relies on pre-trained DL models, which may pose challenges in memory retrieval settings.

Ali et al. [24] presented a novel method for identifying monkeypox skin lesions using deep learning models. They utilized the freely available "Monkeypox Skin Lesion Dataset (MSLD)" for automated monkeypox detection using skin lesions images. They employing cutting-edge DL approaches such as VGG16, ResNet50, and InceptionV3, along with transfer learning strategies. They anticipate that their approach could offer new avenues for researchers developing computer-aided diagnostic tools that can be deployed remotely for rapid testing and early diagnosis of monkeypox, particularly in scenarios where traditional testing methods are impractical.

In the study mentioned, they use deep learning to pick out important features and swarm intelligence to classify images. This method works fast and fits well on smartphones. They also suggest using a special kind of Swarm Optimization approach called binary PSO and pertained deep learning approaches are pick the best features for training an image classifier [25, 26 and 27].

3.0 DATASETS AND METHODS

3.1 Dataset

In this study, we use the freely available Monkeypox image dataset ISIC [28, 29]. The dataset is separated into subfolders, with and without augmentations. In our study, we use augmented images because deep learning models favor them for learning critical information more accurately. The number of images from the expanded database in each category is shown in Table 1.

Table 1: The frequency of cross-validation images per class

Class	Image validation	Images for training purposes	Images with augmentation
Monkeypox	389	1234	(1234*19=) 23,446
Chickenpox	267	840	(840*12=) 10,080
Smallpox	185	653	(653*9=) 8,489
Cowpox	135	468	(468*17=) 7,956
Measles	123	375	(375*19=) 7,125
Tomato Flu	82	275	(275*17=) 4,675
Normal	335	1080	(1080*19=) 20,520

3.1.1 Data Collection

Web crawling to collect images: We collect images of skin infected by monkeypox, chickenpox, smallpox, cowpox, the tomato flu, and measles, as well as healthy skin images, using internet and different search engine. We searched for images with "open source licenses." Images for certain pox classes are challenging to obtain. As a consequence, we collect photographs with "commercial and other licenses." As a result, we share extra information for all of our collected photos, such as the source's universal resource locator (URL), the date of access, and the image credit (if applicable) [19]. Figure 1 depicts some photos within our database.

Fig. 1: Examples of skin images from our dataset

Expert Screening: In expert screening examined all of the photos collected to evaluate the probable disease, then we applied thorough analysis techniques, leveraging medical expertise to accurately assess the condition depicted in Fig. 1 & 2 and shows an illustration of our dataset's original training image percentages in a pie chart per category of images. This involved scrutinizing details such as symptoms, lesion characteristics, and other relevant indicators to make informed evaluations. Additionally, we utilized advanced diagnostic tools and algorithms to augment the screening process, enhancing accuracy and efficiency. Our comprehensive approach ensured that all potential disease cases were identified and categorized correctly, contributing to the reliability and effectiveness of our dataset for further research and analysis.

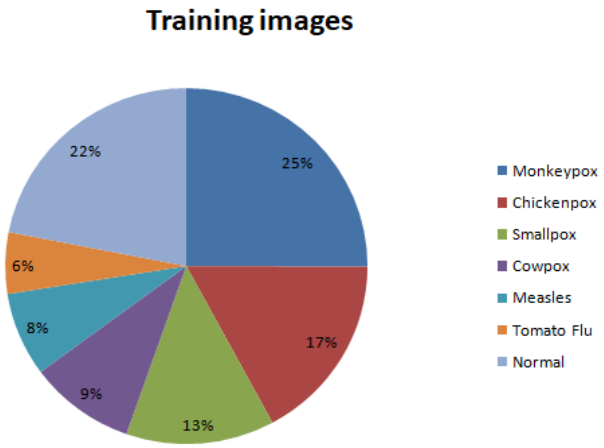

Fig. 2: The percent of original training images per class in our dataset

Data Preparation: We reduced image sizes to unnecessary backdrop areas and make patients more problematic, the ocular region was restricted with black boxes to distinguish from identical images [28]. We applied the same technique to exposed private areas. Due to the fact that many AI deep models input square-shaped images with high pixel counts (typically 299×299×3 pixels), In order to avoid the actual skin lesions from being too expanded during image scaling, we placed extra blank pixels around the edges of some images.
Expansions: To increase the number of photos we introduce instability to the data that used the Python Imaging Library (PIL) version 9.3.0, the Scikit-Image library version 0.19.3, and the Tensor Flow Library version 2.10.0 to perform different augmentation operations on web-scraped images.

3.2 Evaluation Metrics

We use four common performance metrics: precision (P), recall (R), F1-score (F), and accuracy (A) [28, 30].

$$\text{Precision (p)} = \frac{T_P}{T_P+F_P} \tag{1}$$

$$\text{Recall(R)} = \frac{T_P}{T_P+F_N} \tag{2}$$

$$F_1\text{-Score} = 2\times \frac{Precision(P)\times Recall(R)}{Precision(P)+ Recall(R)} \tag{3}$$

$$\text{Accuracy (A)} = \frac{T_P+T_N}{T_P+T_N+F_P+F_N} \tag{4}$$

True positive, true negative, false positive, and false negative are denoted, respectively, by the symbols TP, TN, FP, and FN.

3.3 Pre-trained DL Models

Many researchers have already developed many techniques; in this research, we examined and compared our dataset with previously developed models, which are discussed below:
VGG16: The Oxford University's Visual Geometry Group (VGG) [31] created the VGG-16 Convolutional Neural Network (CNN), which was successful in the 2014, ImageNet [22] test. Three dense layers, five maximum pooling layers, and 13 convolutions make up this structure. The term VGG-16 refers to the fact that it contains 16 layers with learnable weight values. 16 convolution layers are present in the enhanced VGG-16 model in ImageNet.
ResNet50: In an image classification task on a large scale, the incredibly deep convolutional neural networks VGG-16 and VGG-19 demonstrated outstanding results. The vanishing gradient problem, which occurs when the multiplication of weak gradients transmitted back to the preceding layer starts to decrease at a specific depth, makes it difficult to train an unusually deep neural network. By creating the notion of a skip connection, which enables the network to be built without some layers, the scientist attempted to solve the vanishing gradient problem. Residual blocks (Res-Blocks), which form the foundation of the ResNet design, are a subset of the network layers that take advantage of these hidden neurons. Two ResNet designs are used in this context: ResNet-50[31]. One Maxpooling layer, one average layer, and 48 convolution layers make up the ResNet-50.

Inception V3: A team of Google researchers adopted the notion of broadening the network rather than deepening it in the Inception network [32]. The Inception network architecture collects visual input at multiple scales before passing it on to the following layer using different kernel sizes with four concurrent convolutional layers at a certain network depth. In this scenario, we implement an Inception-v3 network with 48 layers.
Ensemble models: An ensemble is a group of things that are seen collectively rather than individually [33]. An issue is solved using an ensemble approach, which creates several models and merges them. The durability and generalizability of the model are enhanced by ensemble techniques. The use of ensemble approaches is common in conventional machine learning. Random forest and the bagging meta-estimator are examples of bagging algorithms, whereas GBM, XGBM, Adaboost, and other boosting techniques are examples of boosting techniques.

- **Stacking:** It is an ensemble approach that uses a meta-model to include multiple models (classification or regression, meta-classifier, or meta-regression). The basic models are trained on the complete dataset, whereas the meta-model is trained on the base models' output characteristics. Typically, stacking employs many basic models. To achieve the best degree of accuracy, the meta-model helps determine the features of base models.
- **Blending:** It is similar to the stacking technique discussed above, but instead of using the complete dataset to train the basic models, a validation dataset is kept separate to create predictions.
- **Bagging:** It is also known as a bootstrapping technique. Base models are performed on bags to ensure that the entire dataset has a balanced distribution A sack is a set of a dataset that has a replacement that increases the size of the sack to the size of the entire dataset.
- **Boosting:** Boosting is a sequential technique that attempts to protect the outcome from being influenced by an incorrect base model.

3.4 The Proposed Approach

Several segmentation approaches have been developed to automatically discover and diagnose skin lesions in images, some of which are for traditional macroscopic images and others for dermoscopy images. The identification of monkeypox skin lesions is accomplished using particle swarm optimization, GLCM, and the Hidden Markov Model (HMM) [34]. Figure 3 depicts the application of particle swarm optimization for monkeypox image classification with the GLCM [35] to retrieve image features using SVM classifier [36]. Our techniques have three components that are feature extraction, feature selection, and classification. A GLCM is extremely effective for retrieving information from raw colour images. Then we trained one such DL-models for example ResNet50 [31], to extract features from input images using SVM classifier. ResNet50's nonlinear activation layer is eliminated, and features are reconstructed by considering the results of 100 nodes'. PSO is used to choose features from the 100 extracted ResNet50 features. We investigated using a binary selection to represent each parameter in PSO. This provides us with a given dataset from which to select a population size of 100, ranging from 1 to 4,925. The velocity and parameters were modified using the multi-objective fitness function based on the global and local bests of each particle. We set the confidence range of the swarm and the self-confidence range of the velocity function to 0.80 [25]. After experimenting with various settings, these parameters were selected to produce the best results. We receive the necessary number of features while our GLCM-SVM classifier is being trained (Fig. 3).

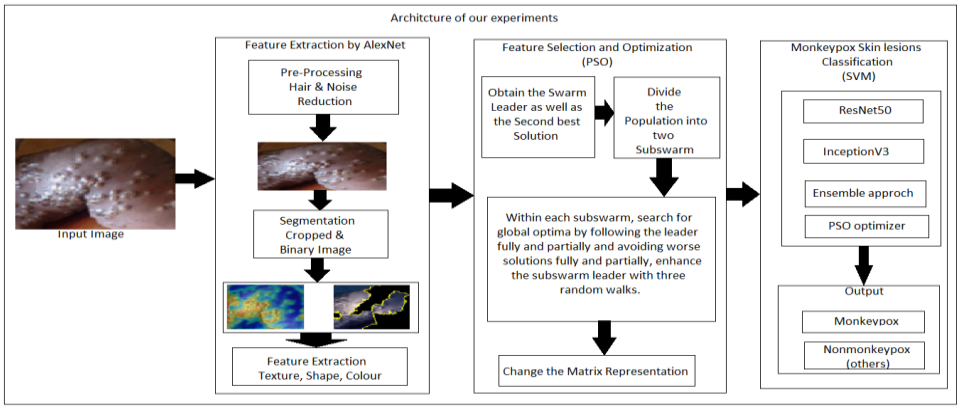

Fig. 3: The architecture of our experiment monkeypox virus detection

3.4.1 Feature Extraction

The extraction of features is crucial to extracting information from a given image. The analysis of previous layers will make use of GLCM. To record the spatial dependency of image pixels, the GLCM method is applied. Using a gray-level image matrix, GLCM captures the most common features, including contrast, mean, energy, and homogeneity [34, 35]. Any detection or identification system's performance is greatly impacted by the attributes acquired. Since the dataset wasn't big enough to training a neural network for the necessary level right away, deep learning was applied. By modifying the existing model, deep learning improves training. The classification function uses a softmax classifier to determine the 1,000 class probability by the ImageNet dataset in the original ResNet50 model. Using ResNet-50, 48 convolutional layers, 1 Maxpooling layer, and 1 average pooling layer make up ResNet-50. Based on the findings of the previous layer as well, a prediction is generated in the final fully connected layer. The weights of the preceding layer are reset in order to train the supervised learning model on the new dataset because it was learned on a different dataset. We reduce the class size to 100; this is the model's minimum number of features, because ResNet produces a 1000-way SoftMax output. These 100 classes' output is employed as a feature. In feature extraction, by reducing the number of classes, it potentially improves prediction performance. This is because reducing the number of classes can help in simplifying the classification problem, making it easier for the model to learn and generalize patterns from the data. With fewer classes, the model may encounter less complexity and ambiguity, leading to more accurate predictions.

3.4.2 Feature Selection

The goal of PSO is to choose the most efficient feature subset from all of the collected features. Every particle in the population stands in for a prospective candidate for a solution. The fitness function enables evolution, which also forecasts fitness in upcoming trials. Every particle was initially constructed according to a binary alphabetic string $Z = f_1f_2f_3f_4...f_m$, m = 1, 2, 3, 4,... z, where "z" is the length of the recovered feature vector, in this case 100, and "m" is the number of particles. Which feature is selected depends on each index of the binary input; "1" represents the selected feature, while "0" signals rejection. In the search area denoted by 2z, the algorithm searches for the best solution. For example, we can choose any group of the features less than m when using PSO to assess a 10-dimensional dataset (n = 10). For instance, in PSO, the proposed approach can choose six features at random [$f_2f_3f_5f_7f_9f_{10}$] by setting bits 2, 3, 5, 7, 9, and 10. In order to retain the maximum level of accuracy and accurately represent the original feature set for each particle, the fitness value is used to assess exactly how well the chosen feature subset works. The values represented by the particle's feature Z are the parameters that the PSO will repeatedly regenerate. The fitness function "f" determines the fitness or quality value for each particle in each iteration. The fitness function stimulates this creation and evaluates the quality of generated particles based on their ability to improve prediction performance. When training the classifier using the particle's data, the fitness function employs a k-fold cross-validation function with k = 10. As a fitness value for evolution, the classifier's accuracy is employed.

3.4.3 Classification

A classifier is used to identify images of monkeypox skin lesions from those of other skin diseases. The hidden Markov model (HMM) classifier is employed for simplicity. HMM analyses a set of images and predicts which of two categories of monkeypox skin lesions and other classes each input image relates to, a statistical Markov model known as the HMM implies that the system is a Markov process with unobservable (i.e., hidden) states. In our proposed approach, the GLCM output is entered into an HMM [34, 35]classifier along with an SVM [36], which accepts training data, testing data, and grouping information to determine if a particular input picture contains monkeypox skin lesions or other skin diseases. Then final step is to categorize the picture into several illness classifications. The classifier is trained using the best set of features that PSO determined from the attributes that ResNet50 had recovered. Support Vector Machine (SVM), VGG16, InceptionV3, and the Ensemble approach, among other classifiers, were tested for cross-validation accuracy; SVM was chosen for picture categorization (Fig. 3).

4.0 PSO MODEL FOR DIGITAL IMAGES SELECTION

This section outlines the proposed model for identifying and diagnosing the monkey pox virus. The identification of monkeypox skin lesions is accomplished through the use of PSO, GLCM, and the hidden

markov model (HMM) with an SVM classifier. The PSO clustering technique is used in this paper to accurately diagnose monkey pox. A new variant of PSO is proposed in this paper to assess the most important diagnostic findings of healthy and diseased skin lesions. To prevent the basic PSO model from emerging too early, it contains partial and complete attract and flee operations, mutation-based local exploitation, and alternative matrix representations. Each particle can follow multiple swarm leaders, avoid local and global worst particles, and search internally or externally for the global best solution to find them according to the proposed model. The proposed method is effective in selecting feature classifiers and obtaining the best overall result. The following sections discuss both the old and new PSO models.

4.1 Feature Extraction using GLCM

The feature extraction strategy utilizing the Gray Level Co-occurrence Matrix (GLCM) [34, 35] is centered on constructing this matrix across the entirety of the infected skin image, a task made intricate due to the presence of diverse clinical structures, including various skin infections that pose a formidable challenge in detecting exudates. In this section, an innovative method is introduced where the input image is segmented into smaller blocks of 9x9 pixels and categorized into four distinct groups based on their content: Blocks I: = 0^0, Blocks II: = 45^0, Blocks III: = 90^0 , and Blocks IV: = 135^0, for each RGB image feature. Following this categorization, both first-order and second-order characteristics are extracted from these blocks.

The GLCM is a fundamental component of this process. It's essentially a matrix that is sized to match the number of gray levels in the image, denoted as 'G.' Each entry in the matrix, labeled as P(l, m | Δx, Δy), indicates how often two pixels with intensities 'l' and 'm' are found within a defined neighborhood distance (Δx, Δy) of each other. In a similar context, the matrix element P(l, m | d, Θ) represents statistical probabilities that describe the connections between gray levels 'l' and 'm' at a precise displacement distance 'd' and angle (Θ). It's worth emphasizing that GLCMs are notably influenced by the dimensions of the texture samples employed in their computation [37, 38]. Consequently, for the enhancement of GLCM construction, it is common practice to decrease the number of gray levels.

Subsequently, feature extraction is conducted based on the constructed GLCM, encompassing various intensity features like contract, homogeneity, angular second moment, energy, and correlation derived from color retinal images. The third phase is feature extraction, during which the GLCM model is employed to extract features from the skin image. The GLCM algorithm is applied to perform feature extraction specifically to capture the textural characteristics of the input image. The GLCM algorithm plays a pivotal role in extracting image features for the detection of skin rashes. The extracted features, which are dependent on the GLCM from the input image, are as follows [37]:

$$\text{Contrast } = \sum_{l=0}^{N-1}\sum_{m=0}^{n-1}(l-m)^2 \tag{5}$$

$$\text{Homogeneity} = \sum_{l=0}^{N-1}\sum_{m=0}^{N-1}\frac{P(l,m)}{1+(l-m)^2} \tag{6}$$

$$\text{Dissimilarity} = \sum_{l=0}^{N-1}\sum_{m=0}^{N-1}P(l,m)x|l-m| \tag{7}$$

$$\textit{A}\text{ngular second Moment} = \sum_{l=0}^{N-1}\sum_{m=0}^{N-1}P(l,m)^2 \tag{8}$$

$$\text{Energy} = \sqrt{\sum_{l=0}^{N-1}\sum_{m=0}^{N-1}P(l,m)^2} \tag{9}$$

$$\text{Correlation} = \sum_{l=0}^{N-1}\sum_{m=0}^{N-1}\frac{(l-\mu_l)(m-\mu_m)}{\sqrt{\sigma_l\sigma_m}} \tag{10}$$

4.2 Classification of Image using SVM

The support vector machine (SVM) classifier [36] will be utilized to distinguish between defective and non-defective regions in the skin. This classifier is adept at identifying the percentage of defective area, making it an effective tool for regression, classification, and general pattern recognition. Hence, it is commonly referred to as the SVM classifier. It boasts excellent generalization performance, even when confronted with high-dimensional input spaces, all without the need for prior knowledge. The core concept involves identifying the optimal hyperplane that effectively segregates one class from the other, with the "best" hyperplane maximizing the margin, signifying the broadest separation between the two classes. This margin represents the maximal space width parallel to the hyperplane without any internal data points. In this chapter SVM models transform data into a representation where examples from distinct categories are distinctly separated by infected and non-infected images. Consequently, the skin images are mapped into the same space and classified based on their positioning relative to this skin images, rendering SVMs invaluable for tasks like distinguishing infected from non-infected images. This classifier stands out as one of the best options among all classifiers and is well-suited for binary classification as well as resolving multiclass issues.

4.3 Proposed Search Strategies

The hidden Markov model and SVM are used in the diagnostic test to separate monkeypox skin lesions from other skin infections. Digital image processing methods and particle swarm optimization are also used for image classification. The information from an image may be used for analysis and retrieved using the GLCM. In the previous stage, 100 features for each picture were extracted using the GLCM. In light of the computational complexity of the previous step, an optimization strategy that can find the most significant or remarkable features is required. PSO, a heuristic technique, is used to discover the best collection of features. The social activities of fish schooling and bird flocking use to develop PSO. The primary idea of PSO is that social interaction with the population improves intelligence, which takes into account both the individual and collective behavior of birds [25, 26 and 27]. In PSO, each solution may be considered a distinct particle. $P_i = (P_{i1}, P_{i2},\ldots, P_{iN})$, where N is the vector's dimension, is used to represent the particle's location within the search space. The optimal solutions at a specific velocity are determined by updating each particle in the search space, which is indicated by the notation $V_i = (V_{i1}, V_{i2},... V_{iN})$. Each particle changes its location and speed during this stage. The variable "p_{best}" represents the particle's best recent location, whereas "g_{best}" reflects the population's best position. PSO chooses the best options based on the parameter values pbest and gbest by updating each particle's location and velocity using the following equations:

$$v_{i,j}^{t+1} = w.\, v_{i,j}^{t} + c_1 r_1 (p_{best}^{t} - p_{i,j}^{t}) + c_2 r_2 (g_{best}^{t} - p_{i,j}^{t}) \quad (11)$$

$$p_{i,j}^{t+1} = p_{i,j}^{t} + v_{i,j}^{t+1} \quad (12)$$

Where "t" indicates the iteration counter, XP_{best} is the particle's best position on the jth dimension, Xg_{best} is the g_{best} position, v_{ij} is the particle's velocity on the j^{th} dimension, whose value is limited to the range $[v_{min}; v_{max}]$, P_{ij} is its position on the j^{th} dimension. Global search and local exploitation are controlled using the inertia weight "w." The range of the random variables r_1 and r_2 is [0, 1], and the velocity weight is typically set to 1 using the constraint factor b. The values of the personal positive constants c_1 and c_2, as well as the social learning factors, are 1.

4.4 PSOMPX Algorithm Descriptions

This article presents Particle Swarm Optimization Monkeypox (PSOMPX) for skin lesion identification using the Hidden Markov Model (HMM) and GLCM-SVM classifier. The image of the skin lesion is sent into the system, where it is processed through several pre-processing procedures for noise reduction and image enhancement. Using the PSO technique, the image is then exposed to division. The GLCM system must be used to extract a few image highlights. These highlights are supplied as input to the SVM-classifier. The suggested PSO variant is described using the Hidden Markov Model (HMM), which comprises local exploitation and attraction based on mutation, global evasion-driven exploration, and the sub-swarm approach to reduce local optimal traps. To continue, a basic swarm of 100 particles is generated. After that, the particles are arranged according to their fitness ratings. The worst solutions and the world's worst leader are correspondingly stored in the best and worst memory structures. It is possible to find a better appropriate secondary swarm leader that is less connected to the primary one. The primary swarm then separates into two smaller groups. Each sub-swarm is given one of the two swarm leaders to direct the search operation.

The original PSO velocity update method is applied if a single particle in a sub-swarm is one of the worst particles that have been previously detected and kept in memory. For position updates in each dimension, it fully follows the sub-swarm leader, as defined in Equations (5) and (6). Otherwise, the algorithm employs the four methods listed below before finally using the operation that produces the best result to control the search process, i.e.,

- The first PSO algorithm [25, 26] states that in every dimension, every particle completely follows the leader.
- The leaders of the sub-dimensions are chosen at random, and the others follow.
- It prevents the worst possible personal and global experiences in every dimension.
- It chooses a few sub-dimensions at random and avoids the worst folks in those dimensions both locally and globally.

These four search methods help to expand the search process as well as the proposed PSO model to analyze other search areas while decreasing the chance of being affected by local optima. Each particle uses one of the four techniques to update its position during the search. The four actions' primary offspring are then used to update velocity. Each subpopulation has a new sub-swarm leader after a certain number of cycles. By using the

Gaussian, Cauchy, and Levy probability distributions, the new sub-swarm leader is significantly enhanced. If the child solution generated by any of these nonlinear processes performs better in terms of fitness than the existing parent sub-swarm leader, the parent sub-swarm leader is replaced by the promising offspring. After the two subpopulations have merged, the best solution from the two sub-swarm leaders is selected as the new global best solution. The worst record is updated using a unique combination of these solutions.

The above-mentioned search operations are performed solely with the primary swarm rather than two sub-swarms if the second swarm leader, which has a promising fitness score but a low correlation to the global best solution, cannot be positioned at the start of the search process in a fixed number of iterations. After that, the search process is restarted using an updated matrix representation generated by dynamically changing the current matrix's rows and columns, which changed the particle-matrix representation from 10×20 to 20×10. The algorithm iterates until the termination requirements are satisfied.

5.0 ANALYSIS OF EXPERIMENTAL RESULTS

The following are the overall steps of our experiments:

- We use a database of skin lesion or rash photos from six distinct diseases (as compare to three in [28]), which include monkeypox, chickenpox, smallpox, cowpox, measles, and tomato flu, as well as images of normal skin.
- Our dataset has more information for measles, pox, and healthy images that were downloaded from the Internet (i.e., 4925 photographs) than previous comparable datasets used in [39, 40]. (1234 and 1080 images of monkeypox skin lesions and healthy skin images, respectively).
- We evaluated the efficacy of four state-of-the-art deep learning models for diseases classification using digital skin images (comparison to one and three deep learning models in [34, 35]). Performances in classifying diseases for VGG16 [31], ResNet50 [31], Inception-V3 [32], and Ensemble [33] were examined.
- Although their dataset was smaller than ours, we conducted 10-fold cross-validation tests on each of the PSOMPX models to more thoroughly examine our results.

The database collection has 4925 photos separated into 7 groups, which include both sick and healthy skin images of the human body. Table 1 illustrates the seven classes and the number of photos used in each class. Our model was trained with around 703 photos of each class using a 65%-35% Splitting train-cross validation to test the performance of the suggested strategy on a unique dataset and to keep track of the classifier in our approach. The testing dataset had 69 photos for each of the seven classes, for a total of 483 images.

Table 2: Different Classifiers cross-validation test result analysis

Classifier	Accuracy	Precision	Recal	F1-Score
PSO Optimizer	90.01	86.16	85.58	85.87
VGG16	82.94	80.18	79.17	79.68
ResNet50	84.87	82.81	81.60	82.20
Inception V_3	84.53	82.51	82.30	82.40
Ensemble	87.13	85.44	85.47	85.46

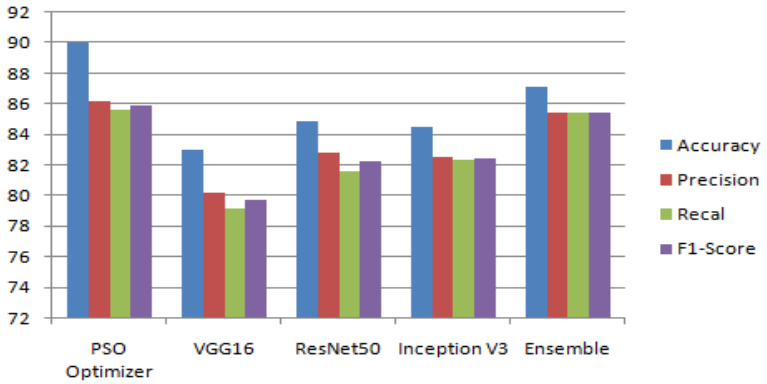

Fig. 4: Performance comparison of accuracy, precision, Recall, F1-Score

After building the classifier for seven classes, 100 features were obtained. The 24 best features were gathered and used to train our classifier using PSO, GLCM-SVM classifier, and the Hidden Markov Model (HMM). Approximately 4925 photos were used for training the ResNet50 feature extraction model for seven classes; while Cross-validation was performed using 1516 images. The ratio of cross-validation to training was 65% to 35%. A total of 4,925 images were used to train the model. Table 2 displays the accuracy and performance metrics obtained for the specified number of iterations. Each image has 100 characteristics extracted. From the 100 features collected using binary PSO that was used to choose the best feature subset. The values of the PSO parameters are depicts below in Table 3.

Table 3: PSO Parameters Setting

Population	100
Error Criterion	0.01
C_1	1.00
C_2	1.00

Table 4: Results of the PSO optimizer

g_{best} fitness	0.978
g_{best}	6621208546588 7782960042360860
Iteration	101

The PSO findings are summarized in Table 4, and the "g_{best}" fitness value offers the global best fitness value as well as the optimum global parameter, which relates to the best subgroup. The global best argument, defines which column must be chosen when converted to binary. The binary equivalents of 6621208546588 7782960042360860 are: 1101010111110001010110100111100101011000011101110101110101101001000 111101011111 000100000000011100. The 24 features with indices of '1', '3', '5', '7', '8', '10', '17', '20', '21', '25', '27', '28', '29', '31', '34', '37', '41', '44', '48', '50', '55', '58', '67', '69' were used for feature selection. The classifier was trained using this ideal set of attributes of PSO+GLCM-SVM classifier. The cross-validation results for well-known DL- classifiers are shown in Figure 4 in terms of accuracy, precision, recall, and F1- score. The following classifiers: On the basis of their cross-validation F1-scores, the PSO classifier, VGG16, ResNet50, Inception V3, and Ensemble are compared. PSO classifier was chosen for classification because, with an F1-score of 85.87%, it performed better than the other classifiers. The ideal feature subset, which consists of 24 features, was used to train the PSO Optimizer classifier. Only 9 images out of a total of 4925 were correctly classified, with 69 images from each class being included in the testing. As a result, a total accuracy of 90.01% (F1-Score: 85.87%) was achieved. The classification's full findings are presented in Table 2 and Figure 4. The precision, recall, and F1-score for each class are evaluated, giving an F1-score of 85.87%. The Precision-Recall result comparison for the test data using pertained DL Models and PSO Optimizer was shown in Figure 5 which created using the information from Table 2's results.

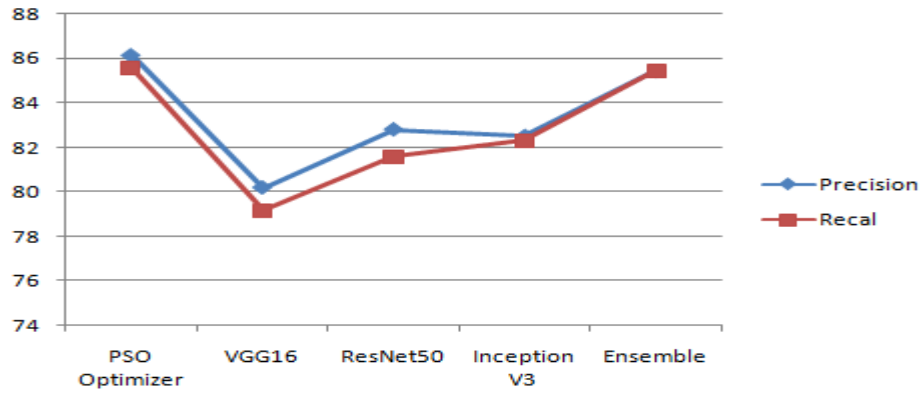

Fig. 5: Precision-Recall result comparison for the test data using pertained DL Models and PSO Optimizer

The outcomes of this approach are similar to those of the one-versus-rest technique when used directly. The available constraints, such as the required precision, the time allotted for development, the processing time, and the nature of the classification problem, will define the strategy to be used in practical situations. Figure 6 shows the accuracy and loss training and test curves for the PSO optimizer. Finally, employing image processing methods and a machine learning application, the experimental findings demonstrated (in Figure 7) an automated

detection of monkeypox lesions. Image capturing and extraction, image preprocessing, feature extraction, feature selection, and classification are all parts of it. The development of an autonomous detection system using cutting-edge information techniques, such as image processing, that helps clinicians identify infections early and gives crucial data for virus management.

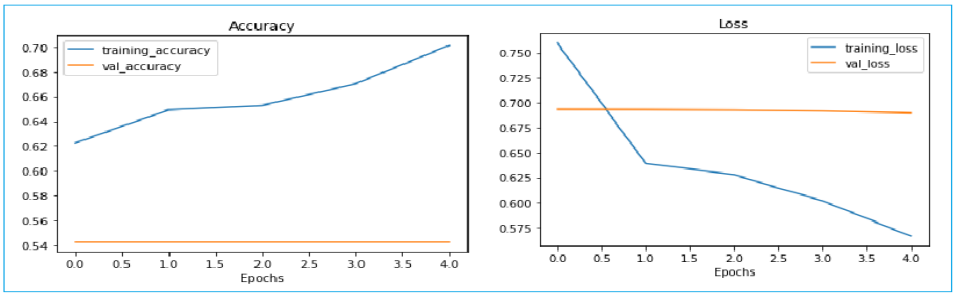

Fig. 6: PSO optimizer sample train/test plot for accuracy and loss

Results:

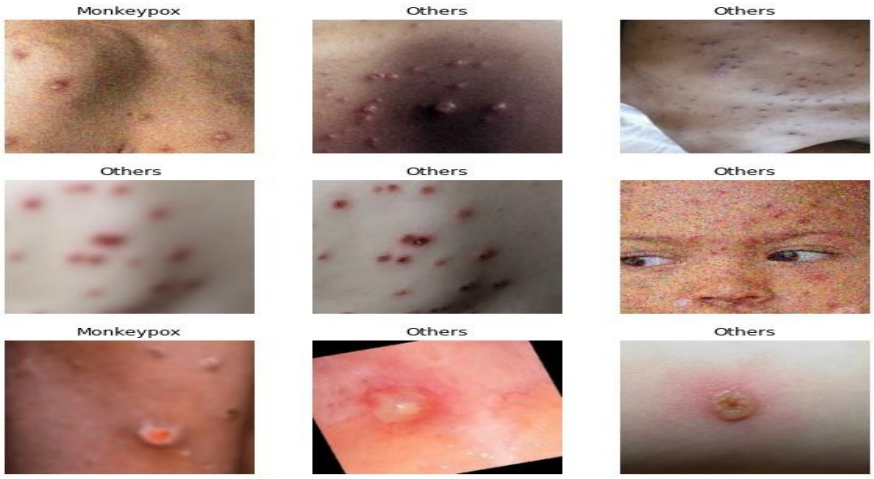

Fig. 7: Visualization results based on PSO optimizer with image categorization using GLCM-SVM Classifier

5.1 Comparative Analysis with State-of-the-Art Method

In this article, a novel hybrid strategy is introduced, harnessing the power of Particle Swarm Optimization (PSO) to improve the accuracy of MPX detection from skin lesion images. In this subsection, a comparative analysis is carried out to contrast the proposed model's results with a cutting-edge pretrained deep learning approach found in the state-of-the-art literature. The method used for benchmarking is the XGBoost and Random Forest technique by Farzipour et al. (2023) [41], driven by the latter's strong performance, facilitating a comprehensive evaluation of the proposed strategy's effectiveness. The results of these comparisons are visually presented in Table 5 and Figure 8, demonstrating that the proposed PSO-based Monkeypox detection strategy—referred to as PSOMPX—has outperformed Farzipour et al. (2023) [41] in respect of all measured metrics. This impressive performance gain can be attributed to a pivotal element within this strategy. To assess the effectiveness of this classification, the results are validated using a confusion matrix for the calculation of accuracy, F1-score, precision, and recall. An inherent limitation of the method [20, 28] is that it only experiments with two pretrained deep learning models. This particular choice leads to the untimely exclusion of prospective candidate classes in the initial phases, thereby detrimentally impacting the process of decision-making. As a result, the integration of the proposed PSOMPX approach with GLCM-SVM and the innovative normalization process yields superior results when compared to the existing state-of-the-art method. This comparative analysis underscores the effectiveness of the suggested strategy in accurately detecting Monkeypox from skin lesion images.

Table 5: Comparison of PSOMPX performance measures with Farzipour et al. (2023) [41]

Models	Precision	Recall	F1-Score	Accuracy
PSOMPX	86.16	85.58	85.87	90.01
XGBoost [41]	86.80	90.00	86.40	90.00
Random Forest [41]	86.40	87.70	85.40	87.70

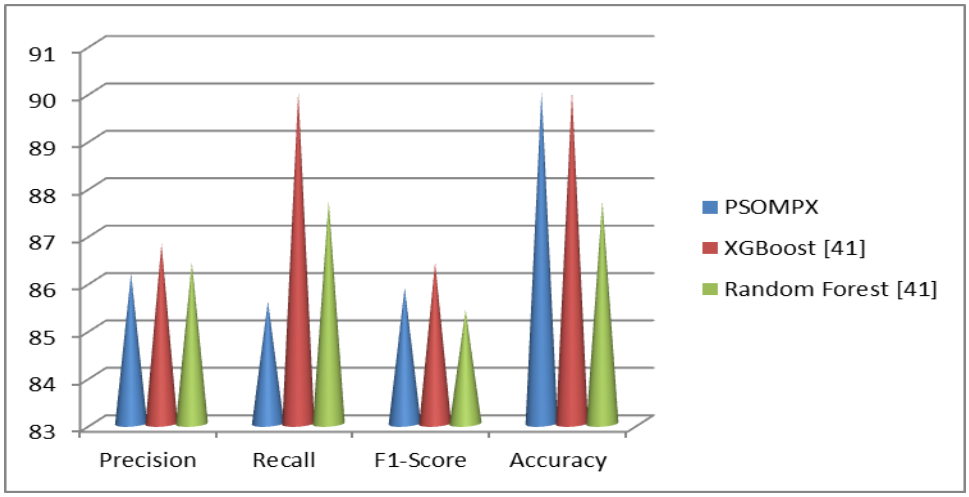

Fig. 8: Comparative Analysis with State-of-the-Art Method

5.2 Discussion

The research presented in this study showcases the efficacy of bio-inspired techniques, particularly Particle Swarm Optimization (PSO), in the realm of medical image analysis, with a focus on the identification and diagnosis of monkeypox virus. By integrating PSO with machine learning classifiers, such as GLCM-SVM and compare proposed model experiment results with existing deep learning models ResNet50, VGG16, and InceptionV3. In conclusion, the proposed PSOMPX method demonstrated superior performance in accurately identifying monkeypox cases from digital skin images. One notable aspect of this study is the utilization of the International Skin Imaging Collaboration (ISIC) dataset, which comprises various skin conditions, including monkeypox, chickenpox, smallpox, cowpox, measles, tomato flu, and normal skin. This diverse dataset allowed for comprehensive experimentation and validation of the PSOMPX method across multiple skin conditions, ensuring its robustness and applicability in real-world scenarios. The application of a hidden Markov model (HMM) in the diagnostic process further enhances the accuracy of distinguishing monkeypox lesions from other skin conditions. Additionally, digital image processing techniques, combined with PSO for image segmentation, contribute to the extraction of relevant features for classification, thereby improving the overall performance of the PSOMPX method. The article also highlights the potential impact of the proposed approach on medical diagnosis and public health. By enabling remote, computer-aided diagnostic techniques, individuals can conduct preliminary examinations for monkeypox from their homes, facilitating early detection and timely intervention. This capability becomes particularly valuable in situations where traditional testing procedures are inaccessible or impractical.

Furthermore, the evaluation of the proposed approach using a comprehensive set of performance metrics, including accuracy, precision, recall, and F1-score, reaffirms the superiority of the PSOMPX method over existing approaches. Graphical representations of the experimental findings provide visual evidence of the effectiveness and durability of the proposed techniques, and their practical relevance in clinical settings.

6.0 CONCLUSION

The proposed methods in this research increased the accuracy of the identification of cases of monkeypox in images. A hidden Markov model is used in the diagnostic process to differentiate monkeypox skin lesions from other skin conditions, as well as digital image processing methods and PSO for picture segmentation. Images are processed to extract characteristics that may be classified using the PSO+GLCM-SVM classifier. The PSOMPX method, a hybrid of PSO algorithms, aims at identifying the optimal collection of features to improve

classification accuracy. The proposed methods are assessed using a publicly accessible monkeypox dataset that has been improved to match transfer learning using ResNet50 [31], VGG16 (AVGG) [31], InceptionV3 [32], and the ensemble approach [33]. We anticipate that this work will provide ample scope for research into remotely deployable computer-aided diagnostic techniques for widespread screening and early monkeypox detection, particularly in situations where traditional testing procedures are not available. In addition, we anticipate that our PSOMPX model will make it feasible for those who think they may have monkeypox to do a preliminary examination from the comfort of their own homes, enabling them to take the necessary action as soon as the condition is detectable. The suggested algorithms were evaluated using two separate sets of criteria. Use a wide range of metrics to evaluate the outcomes as well, for example, the F1-score, accuracy, precision, and recall. The results of the experiment demonstrate the superiority of the proposed PSOMPX model and its collection of features. The durability and effectiveness of the recommended approaches were also illustrated through a series of graphical representations of the findings. The experimental findings show that the suggested algorithms work better than other rival algorithms in the field of classifying monkeypox.
In summary, it is essential to create a smartphone application in future that is user-friendly for the general public as well as physicians, students, researchers, and medical science enthusiasts. The proposed model for disease detection would be included in the application. The scope should be expanded further by including more functionality that provides comprehensive information about skin diseases under one roof.

CRediT Authorship Contribution Statement

Akshaya Kumar Mandal (https://orcid.org/0000-0003-0955-4096): The general idea of literature survey, Data correction, Resources, Implementation, Writing – review & editing – original draft.
Pankaj Kumar Deva Sarma (https://orcid.org/0000-0002-9748-3787): The general idea of literature survey, Review, and editing.

REFERENCES

[1] J.G. Breman, M. Steniowski, E. Zanotto, A. Gromyko, I. Arita. “Human monkeypox, 1970-79”. Bulletin of the World Health Organization 58(2):165, 1980.

[2] L.D. Nolen, L. Osadebe, J. Katomba, J. Likofata, D. Mukadi, B. Monroe, J. Doty, C. M. Hughes, J. Kabamba, J. Malekani. “Extended human-to-human transmission during a monkeypox outbreak in the democratic republic of the congo”. Emerging infectiousdiseases 22(6):1014,2016.

[3] “The World Health Network Declares Monkeypox A Pandemic – Press Release— June 22, 2022,” 2022[Online]. Available: https://www. Worldhealthnetwork.global/monkeypoxpressrelease.

[4] “WHO — Monkeypox Fact Sheet,” 2022, [Online]. Available: https://www.who.int/news-room/fact-sheets/detail/monkeypox.

[5] M. G. Reynolds, G.L. Emerson, E. Pukuta, S. Karhemere, J.J. Muyembe, A. Bikindou, A.M. McCollum, C. Moses, K. Wilkins, H. Zhao. “Detection of human monkeypox in the republicof the congo following intensive community education”. The American Journal of Tropical Medicine and Hygiene 88(5):982,2013.

[6] World health organization (2022) Multi-country monkeypox outbreak: situation update. https:// www. who. int/ emerg encies/ disea se- outbr eak- news/ item/ 2022- DON396. (Accessed: 2022-06-30)

[7] M. A. Hussain, G. Hamarneh, and R. Garbi, “Cascaded regression neural nets for kidney localization and segmentation-free volume estimation,” IEEE Transactions on Medical Imaging, vol. 40, no. 6, pp. 1555–1567, 2021.

[8] M. A. Hussain, A. Amir-Khalili, G. Hamarneh, and R. Abugharbieh, “Segmentation-free kidney localization and volume estimation using aggregated orthogonal decision cnns,” in International Conference on Medical Image Computing and Computer-Assisted Intervention. Springer, 2017, pp. 612–620.

[9] M. A. Hussain, G. Hamarneh, T. W. O’Connell, M. F. Mohammed, and R. Abugharbieh, “Segmentation-free estimation of kidney volumes in ct with dual regression forests,” in International Workshop on Machine Learning in Medical Imaging. Springer, 2016, pp. 156–163.

[10] M. A. Hussain, G. Hamarneh, and R. Garbi, “Noninvasive determination of gene mutations in clear cell renal cell carcinoma using multiple instance decisions aggregated cnn,” in International Conference on Medical Image Computing and Computer-Assisted Intervention. Springer, 2018, pp. 657–665.

[11] M. A. Hussain, G. Hamarneh, and R. Garbi, “Learnable image histograms-based deep radiomics for renal cell carcinoma grading and staging,” Computerized Medical Imaging and Graphics, vol. 90, p. 101924, 2021.

[12] M. A. Hussain, G. Hamarneh, and R. Garbi, “Imhistnet: Learnable image histogram based dnn with application to noninvasive determination of carcinoma grades in ct scans,” in International Conference on Medical Image Computing and Computer-Assisted Intervention. Springer, pp. 130–138, 2019.

[13] M. A. Hussain, G. Hamarneh, and R. Garbi, “Renal cell carcinoma staging with learnable image histogram-based deep neural network,” in International Workshop on Machine Learning in Medical Imaging. Springer, 2019, pp. 533–540.

[14] J. Sun, L. Peng, T. Li, D. Adila, Z. Zaiman, G. B. Melton-Meaux, N. E. Ingraham, E. Murray, D. Boley, S. Switzer et al., “Performance of a chest radiograph ai diagnostic tool for covid-19: A prospective observational study,” Radiology: Artificial Intelligence, vol. 4, no. 4, p. e210217, 2022.

[15] A. Akbarimajd, N. Hoertel, M. A. Hussain, A. A. Neshat, M. Marhamati, M. Bakhtoor, and M. Momeny, “Learning-to-augment incorporated noise-robust deep cnn for detection of covid-19 in noisy x-ray images,” Journal of Computational Science, p. 101763, 2022.

[16] M. Momeny, A. A. Neshat, M. A. Hussain, S. Kia, M. Marhamati, A. Jahanbakhshi, and G. Hamarneh, “Learning-to-augment strategy using noisy and denoised data: Improving generalizability of deep cnn for the detection of covid-19 in x-ray images,” Computers in Biology and Medicine, vol. 136, p. 104704, 2021.

[17] M. Dogucu and M. C, etinkaya-Rundel, “Web scraping in the statistics and data science curriculum: Challenges and opportunities,” Journal of Statistics and Data Science Education, vol. 29, no. sup1, pp. S112–S122, 2021.

[18] T. Islam, M. A. Hussain, F. U. H. Chowdhury, and B. R. Islam, “A web-scraped skin image database of monkeypox, chickenpox, smallpox, cowpox, and measles,” bioRxiv, 2022.

[19] C. Nageswara Rao, S.Sreehari Sastry and K.B.Mahalakshmi “Co-Occurrence Matrix and Its Statistical Features an Approach for Identification Of Phase Transitions Of Mesogens”, International Journal of Innovative Research in Engineering and Technology, Vol. 2, Issue 9, September 2013.

[20] S. Tharangini and G. R. Krishna, "Skin cancer detection using particle swarm optimization," 2018.

[21] T. Y. Tan, L. Zhang, S. C. Neoh, and C. P. Lim, "Intelligent skin cancer detection using enhanced particle swarm optimization," Knowledge-based systems, vol. 158, pp. 118-135, 2018.

[22] G. C. Luh, "A multi-objective particle swarm optimization based threshold approach for skin color detection," in 2013 International Conference on Machine Learning and Cybernetics, 2013, pp. 1114-1119.

[23] S. Chiranjibi and T. B. Shahi, "Monkeypox virus detection using pre-trained deep learning-based approaches," Journal of Medical Systems, vol. 46, no. 11, pp. 1-9, 2022.

[24] S. N. Ali, M. Ahmed, J. Paul, T. Jahan, S. M. Sani, N. Noor, and T. Hasan, "Monkeypox skin lesion detection using deep learning models; A feasibility study," arXiv preprint arXiv:2207.03342, 2022.

[25] J. Kennedy. “The particle swarm: social adaptation of knowledge”. In: Proceedings of the IEEE international conference on evolutionary computation; p.303-308, 1997.

[26] A. K. Mandal, P. K. D. Sarma, and S. Dehuri, "Machine Learning Approaches and Particle Swarm Optimization Based Clustering for the Human Monkeypox Viruses: A Study," in International Conference on Innovations in Intelligent Computing and Communications, Cham, Springer International Publishing, Dec. 2022, pp. 313-332.

[27] A. K. Mandal, P. K. D. Sarma, and S. Dehuri, "A study of bio-inspired computing in bioinformatics: a state-of-the-art literature survey," The Open Bioinformatics Journal, vol. 16, no. 1, 2023.

[28] A.K. Mandal, P.K.D. Sarma, and S. Dehuri, "Image-based Skin Disease Detection and Classification through Bioinspired Machine Learning Approaches," International Journal on Recent and Innovation Trends in Computing and Communication, vol. 12, no. 1, pp. 85-94, 2023.

[29] N. Codella. “International skin imaging collaboration (ISIC)”. In Skin lesion analysis toward melanoma detection: a challenge at the 2017 International Symposium on Biomedical Imaging (ISBI), 2018.

[30] M. Sokolova, N. Japkowicz, and S. Szpakowicz. “Beyond accuracy, F-score and ROC: a family of discriminant measures for performance evaluation”. In Australasian joint conference on artificial intelligence (pp. 1015-1021). Springer, Berlin, Heidelberg, December 2006.

[31] D. Theckedath, and R.R. Sedamkar. “Detecting affect states using VGG16, ResNet50 and SE-ResNet50 networks”. *SN Computer Science*, *1*(2), 1-7.2020.

[32] C. Wang, D. Chen, L. Hao, X. Liu, Y. Zeng, J. Chen, & G. Zhang. “Pulmonary image classification based on inception-v3 transfer learning model”. IEEE Access, 7, 146533-146541, 2019.

[33] T.G. Dietterich. “Ensemble methods in machine learning. In *International workshop on multiple classifier systems”,* Springer, Berlin, Heidelberg, pp. 1-15, 2000.

[34] X. Ou, W. Pan, and p. Xiao. “In vivo skin capacitive imaging analysis by using grey level co-occurrence matrix (GLCM)”. International journal of pharmaceutics, 460(1-2), 28-32 2014.

[35] N.D.N. Nuka, and W.D. Ofor. “Hidden markov model classification scheme for cancer detection in image processing”. Asian Journal Of Multidimensional Research, 11(7), 72-83, 2022.

[36] K. He, X. Zhang, S. Ren, and J. Sun, “Deep residual learning for image recognition,” in Proceedings of the IEEE conference on computer vision and pattern recognition, 2016, pp. 770–778.

[37] T. Islam, M. A. Hussain, F. U. H. Chowdhury, and B. R. Islam, “A web-scraped skin image database of monkeypox, chickenpox, smallpox, cowpox, and measles,” bioRxiv, 2022.

[38] M. M. Ahsan, M. R. Uddin, and S. A. Luna, “Monkeypox image data collection,” arXiv preprint arXiv: 2206.01774, 2022.

[39] S. N. Ali, M. Ahmed, J. Paul, T. Jahan, S. Sani, N. Noor, T. Hasan et al., “Monkeypox skin lesion detection using deep learning models: A feasibility study,” arXiv preprint arXiv:2207.03342, 2022.

[40] P.K. Sethy, S.K. Behera, and N. Kannan. “Categorization of Common Pigmented Skin Lesions (CPSL) using multi-deep features and support vector Machine”. *Journal of Digital Imaging*, 1-10, 2022.

[41] A. Farzipour, R. Elmi, H. Nasiri. "Detection of Monkeypox cases based on symptoms using XGBoost and Shapley additive explanations methods." Diagnostics 13, no. 14 (2023): 2391.